Nanoscale

PAPER

Cite this: *Nanoscale*, 2019, **11**, 2434

Bandgap-controlled hollow polyaniline nanostructures synthesized by Mn-dependent nano-confined polymerization†

Jihye Choi, *[a] Byunghoon Kang,[b] Hyun-Ouk Kim,[b] Jin-Suck Suh,[c] Seungjoo Haam *[b] and Jaemoon Yang*[a,c,d]

Received 18th October 2018,
Accepted 2nd January 2019

DOI: 10.1039/c8nr08420c

rsc.li/nanoscale

Herein, we report a *de novo* synthesis approach to produce bandgap-controlled polyaniline (PAni) nanostructure *via* Mn-mediated oxidative polymerization at the catalytic nanoreactor. To achieve systemic nanoconfined polymerization, manganese oxide (MnOx) nanoparticles coated with silica were used as the sacrificial nanotemplate. Interestingly, the catalytic nanoreactor simultaneously allowed the nanoconfined oxidative polymerization and controlling of the bandgap. MnOx could be reduced by the addition of aniline monomers and consecutive redox reaction at the nanoreactor. Furthermore, core cavity was generated, and ionized Mn could control the bandgap by coordination at the nanostructures.

Introduction

Conducting polymers have numerous interesting photoelectronic properties that vary with their molecular architecture and the extent of π-electron delocalization in the materials.[1–3] One important goal of the current studies on conducting polymers, such as polyaniline (PAni), is to understand the photoelectronic property relationships that may provide the basis for the molecular engineering of polymeric materials for diverse applications in electronics,[4] optoelectronics, photonics, and bioengineering.

Recently, understanding of the photoelectronic properties of PAni has received intense interest due to the unique doping/dedoping behavior,[5] redox properties,[6] intrinsic electrical conductivity,[7] simple synthesis, and favorable environmental stability of PAni. The bandgap of conductive polymers can be controlled by the doping level, which is related to the dopant species and doping method.[8] The most general method for obtaining conducting PAni is chemical oxidative polymerization with ammonium peroxydisulfate in the presence of Brønsted acids,[9] in which the imine nitrogen preferentially gets protonated and the electrical conductivity varies over a wide range as a function of pH from the acid used for doping in the solution-based process.[10] The electrochemical method can support precise doping control; however, it is limited by the PAni film[11] and not suitable for solution processes containing nanoparticulate dispersions. Although the protonation from acids is the simplest way of doping, it is not the only available technique. Interestingly, the other strategy to dope PAni is to utilize metal cations as dopants. Metal ions, such as Li^+, Na^+, Zn^{2+}, Ni^{2+}, Fe^{2+}, Cu^{2+}, or Sn^{2+}, can coordinate to the imine nitrogen atoms of the polymer backbone.[12–14] Based on the results of several experiments involving transition metal salts that can act as the oxidizing agent, Dimitriev *et al.* have proposed the following mechanism: transition metal ions oxidize the amine nitrogen atoms and the reduced metal ions coordinate to the imine nitrogen atoms; then, the reduced cations get oxidized and the imine groups get reduced, yielding doped PAni and oxidized cation.[15] As compared to bare PAni, metal-ion-doped PAni is more attractive for use in optoelectronics, catalysts, color sensors, photothermal therapy, and energy storage owing to its narrower bandgap, enabling absorption in the near-infrared (NIR) light region, reversible color changes, excellent redox property, and relatively high electrical conductivity.[16–18] Indeed, bandgap control is a crucial requirement for utilizing PAni in various applications.

Herein, we demonstrated the systemic nanoconfined synthesis of PAni by controlling the bandgap based on manganese oxide (MnO_x) as the nanotemplate. At first, finely controlled four types of MnO_x nanoparticles were synthesized and were subsequently enveloped by silica shells to formulate catalytic

[a]*Severance Biomedical Science Institute, Yonsei University of College of Medicine, Seoul 03722, Republic of Korea. E-mail: Jihyechoi@yuhs.ac*
[b]*Department of Chemical and Biomolecular Engineering, Yonsei University, Seoul 03722, Republic of Korea. E-mail: haam@yonsei.ac.kr*
[c]*Department of Radiology, College of Medicine, Yonsei University, Seoul 03722, Republic of Korea*
[d]*Systems Molecular Radiology at Yonsei, Yonsei University College of Medicine, Seoul 03722, Republic of Korea*
†Electronic supplementary information (ESI) available. See DOI: 10.1039/c8nr08420c

nanoreactors. MnO_x was reduced into dissolvable Mn ions by the treatment of aniline monomers under the acidic condition and Mn ions could be coordinated from the matrix of PAni during an oxidative polymerization reaction. The morphologies for MnO_x and nanoreactors were assessed by electron microscopy. Subsequently, for the assessment of feasibility for controlling the bandgap of PAni, photonic absorbance and ultraviolet/X-ray photoelectron spectroscopies were conducted to analyze the electronic band structure and density of states for Mn-coordinated hollow PAni (Mn-HPAni) nanostructures.

Materials and methods

Materials

Manganese(II) formate [$Mn(COOH)_2$], oleic acid, trioctylamine, polysorbate-80, tetraethyl orthosilicate, sodium hydroxide, and aniline were purchased from Sigma-Aldrich. Ethyl alcohol (denatured) and toluene (99.8%) were obtained from Samchun Chemical (Republic of Korea). Oleylamine was purified by vacuum distillation over CaH_2. All the other reagents purchased from commercial sources were used as obtained without any further purification. Ultrapure deionized water (DW) was used for all the synthetic processes.

Synthesis of manganese oxide (MnO*x*, I–IV)

$Mn(COOH)_2$ (1.19 mmol), oleic acid (3 mmol), and trioctylamine (3 mmol) were mixed in a 100 mL Schlenk flask equipped with a condenser—connected to a bubbler—and then dried under vacuum at 150 °C for 6 h and backfilled with nitrogen gas. The reaction mixture was subsequently treated with a definitive temperature program. First, the solution was heated to 280 °C for 1 h and then refluxed at 300 °C for changing the color from brownish red to green and then left for 2 h (15 nm), 1.8 h (18 nm), 1.5 h (24 nm), and 1.2 h (38 nm). With the careful exclusion of air and in the presence of water, the slurries remained green after cooling; however, the exposure to air would result in the conversion to a brownish red color. The resulting reaction mixture was cooled to room temperature and the resulting solution was added to excess ethanol (20 mL). Precipitates were formed, which were then isolated by centrifugation at 6000 rpm for 10 min. Oleic-acid-capped MnO_x was obtained as a brown powder.

Synthesis of silica-coated MnO_x (MnO_x@SiO_2, I–IV)

To prepare water-soluble MnO_x@SiO_2, MnO (20 mg) was dissolved in *n*-hexane (4 mL) and then the organic phase was added into 20 mL of the aqueous phase containing 5 mg of polysorbate-80. The mixture was emulsified for 20 min with an ultrasonicator (ULH700S, Ulssohitech, Republic of Korea) at 200 W. After the evaporation of the organic solvent, the products were purified by centrifugation at 18 000 rpm and then the precipitates were redispersed in DW. MnO_x@SiO_2 was then synthesized by the modified Stöber method. MnO_x@SiO_2 was synthesized in a mixture of alcohol and water at ambient temperature using emulsified MnO_x as the seed. Emulsified MnO_x (5 mg) was diluted with ethyl alcohol (3 mL) and 1 mL of 1 M sodium hydroxide solution in DW (60 mL). Further, 100 μL of tetraethyl orthosilicate was added at 20 μL per h; after stirring for 12 h, a silica outer shell was formed on the surface of MnO_x by the hydrolysis and condensation of tetraethyl orthosilicate.

Synthesis of Mn-coordinated hollow polyaniline nanostructure (Mn-HPAni, I–IV)

For the preparation of Mn-HPAni, 10 mg of MnO_x@SiO_2 (I–IV) was added to 1 mL of 1.83 M sulfuric acid and aniline (43.88 mmol). The mixture was vortexed for 20 min and centrifugation was performed two times with excess water. The morphologies were evaluated using a high-resolution transmission electron microscope (TEM, JEM-2100 LAB 6, JEOL Ltd., Japan). To verify the diffraction patterns and elemental composition of the surface, X-ray diffraction (X-ray Diffractometer Ultima3, Rigaku, Japan) and X-ray photoelectron spectroscopy (k-alpha, Thermo Scientific, UK) were used, respectively. Cyclic voltammograms (CompactStat, IVIUM Technologies, USA) were used to estimate the electrochemical properties, and the quantity of Mn ions was determined using inductively coupled plasma optical emission spectrometry (OPTIMA 8300, PerkinElmer, USA). The absorbance spectra were confirmed using a spectrometer (Optizen 2120UV, MECASYS, Republic of Korea). The work functions of Mn-HPAni (I–IV) were measured by an UV photoelectron spectrometer (AXIS Ultra DLD, Kratos, UK).

Results and discussion

For the nanoconfined oxidative polymerization of PAni, four types of MnO_x were synthesized by the thermal decomposition of Mn(II) formate complex using oleic acid as the stabilizer and oxidant. In the transmission electron microscopy image shown in Fig. 1a (left column), the mean diameters of the four types of MnO_x can be determined as 16 ± 1 (I), 21 ± 2 (II), 30 ± 2 (III), and 38 ± 4 (IV) nm (Fig. S1†). To fabricate a stable nanoreactor, oleic-acid-capped MnO_x groups (I–IV) were transferred to an aqueous phase using polysorbate-80 under the basic condition.[19] Subsequently, the formation of silica shells for each MnO_x@SiO_2 (I–IV) as the nanoreactor was achieved *via* the sol–gel reaction of tetraethyl orthosilicate (100, 80, 60, and 40 μL) (Fig. 1a, medium column). By the sequential addition of aniline and sulfuric acid to the MnO_x@SiO_2 (I–IV) nanoreactor, uniform spherical nanostructures (diameter: ~80 nm) with a core cavity were observed in the electron microscopy images (Fig. 1a, right column). Silica shells for Mn-HPAni (I–IV) were darker than those for MnO_x@SiO_2 (I–IV) due to the confined polymerization of PAni. In addition, the core cavities in the middle of Mn-HPAni were observed in all the experimental conditions.

The photonic properties of the synthesized Mn-HPAni (I–IV) using four types of MnO_x were respectively characterized

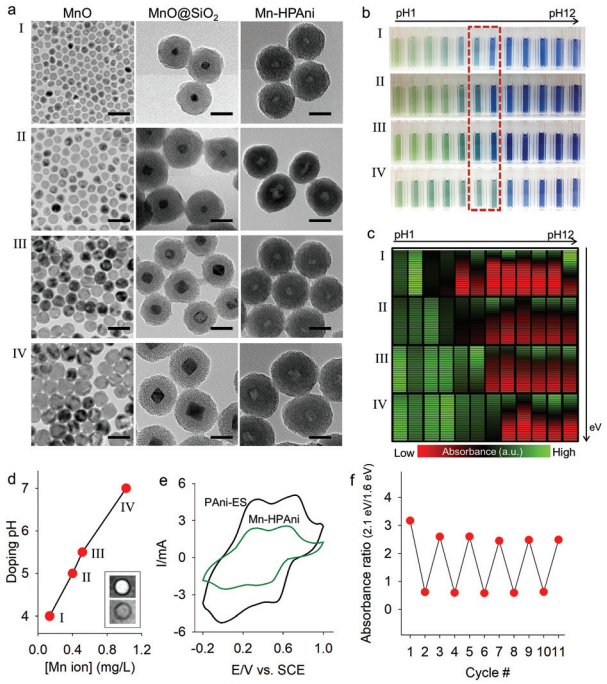

Fig. 1 Precise controlling of nanocavity and bandgap for Mn-HPAni using a catalytic Mn nanoprecursor. (a) Transmission electron microscopy images of four different MnO_x nanoprecursors (I–IV) as the catalytic seeds, silica-coated MnO nanoparticles (MnO_x@SiO_2, I–IV), and Mn-coordinated hollow PAni nanostructures (Mn-HPAni, I–IV). Scale bar: 50 nm. (b) pH-Dependent spectral heat map of Mn-HPAni (I–IV) at various pH values (pH: 1–12). (d) Correlation graph between Mn ions and doping pH. Inset: *T*1-Weighted MR images of Mn-HPAni (IV, upper) and distillated water (lower). (e) Cyclic voltammograms of Mn-HPAni (IV, green line) and PAni in the ES state (black line) electrodes within the potential window from −0.2 to 1 V (*vs.* SCE) at a scan rate of 50 mV s^{-1} in 0.1 M H_2SO_4. (f) Doping/dedoping reversibility from the plasmonic peak using NaOH (1 M) and HCl (1 M) solutions for 11 cycles (n = 5).

at various pH values. As shown in Fig. 1b, the colorimetric change from green to blue was distinct with the increase in pH. In particular, Mn-HPAni (IV) exhibited a green color at neutral pH conditions (dotted red box). To precisely investigate this phenomenon, the absorbance spectra for Mn-HPAni (I–IV) were measured after pH control (Fig. S2†), and their spectral heat maps are shown in Fig. 1c. Due to the difference in the Mn amounts from MnO_x, the absorbance band of Mn-HPAni (I–IV) moved to the near-infrared region with the increase in MnO_x size (IV > III > II > I). That is, the narrowing of the bandgap might result in the electrical conduction state of PAni (emeraldine salt, ES) at neutral pH. To understand the relationship between Mn amount and narrowed bandgap, we quantified Mn ions from MnO_x@SiO_2 (I–IV) using inductively coupled plasma optical emission spectrometry. The amount of Mn was proportional to the critical doping pH related to the narrowed bandgap (Fig. 1d). Moreover, dialyzed Mn-HPAni (IV) exhibited strong R1 relaxivity (3.27 s^{-1}) as compared to distillated water (0.37 s^{-1}) (Fig. 1d, inset) because of the presence of Mn ions in the product. On the other hand, the cyclic voltammograms of Mn-HPAni presented reversible charge–discharge behavior of the composite electrode, like that in PAni-ES. In the case of Mn-HPAni (IV), the first anodic peak appeared at 0.29 V, which was associated with the oxidation of leucoemeraldine to emeraldine. The second anodic peak at 0.84 V was attributed to the emeraldine to pernigraniline transition. Furthermore, Mn-HPAni (IV) maintained the photonic stability under repetitive changes of the pH between pH 1 and pH 12 (Fig. 1f and Fig. S3†). On the other hand, PAni was polymerized using ammonium persulfate in the presence of $MnCl_2$ and the absorbance peak was observed in the near-infrared region (Fig. S4a†). However, there are no specific absorbance peaks under the acidic condition (hydrochloride or sulfuric acid) without extra oxidants (Fig. S4b†). This result implies that the oxide form of Mn, instead of the chloride form, plays the critical role in the polymerization of PAni. The outbreak required for the propagation of the polymeric chains under acidic media requires energy to overcome the barrier created by polymerization. Once this propagation starts, the oxidation potential of the reaction decreases. As a result, the effective nanolocalized polymerization of PAni toward Mn-HPAni was achieved using MnO_x@SiO_2 as the nanoreactor. In the chemical synthesis of PAni, therefore, MnO_x anchored at the nanoreactor was not only used as the nanotemplate, but also regarded as the oxidizing catalyst to facilitate polymerization.

Here, PAni is a dynamic block copolymer consisting of reduced benzenoid units and oxidized quinoid units. Due to the presence of the lone electron pair on the imine and amine sites, emeraldine is regarded as both Brønsted and Lewis bases. Therefore, emeraldine PAni can be doped by Brønsted or Lewis acids at the electron-deficient sites by the formation of coordination bonds.[20] Recently, several Lewis acids have been investigated as dopants for PAni.[12] In particular, Lewis-acid-type doping is extremely important since the complexation of PAni with Lewis acids can significantly alter the band structure of the polymer, yielding important changes in its photoelectrical properties. However, the doping of PAni emeraldine base with Brønsted acids causes the protonation of the imine groups, whereas the amine groups do not participate in this reaction. Therefore, the chemical interaction of PAni with Lewis acids, such as Mn, will be distinctly different from the relationship between PAni and Brønsted acids due to different types of chemical bonds created by the doping process.[21] In addition, it is crucial to investigate the electron band and coordination state of nitrogen atoms from both the amine and imine groups after the acid–base reactions for the produced Mn-HPAni.

To understand the electron state in detail, the density of the valence electronic states were investigated using ultraviolet photoelectron spectroscopy using He I (21.2 eV) and Al-K_α (1486.6 eV) photon lines. The binding energies were calibrated by measuring the Fermi step position and the Au $4f_{7/2}$ core level of a clean gold film. The position of the valence band was determined from the ultraviolet photoelectron spectroscopy data by using the intersection of the linear extrapolation of the leading edge of the valence band spectrum with the base line. The relationship between the energy levels and Mn amounts

from Mn-HPAni (I–IV) is shown in Fig. 2a and 2b. Mn-HPAni (I) displayed the characteristic valence band density of states with the band edge at 4.7 eV. Since the photonic bandgap of Mn-HPAni (I) is 1.3 eV, the conduction band minimum would occur at 3.4 eV. On the other hand, Mn-HPAni (IV) valence band exhibited a notable difference: the maximum energy associated with the band tail blue-shifted further toward the vacuum level at about 4.0 eV. With the increase in Mn, a narrowing of the bandgap occurred and smaller excitation frequencies were expected (Fig. 2c). For the investigation of the coordination state, subsequently, X-ray analysis was conducted. The X-ray diffraction pattern of MnO_x@SiO_2 (IV, grey line) revealed peaks at 2θ values of 35.0°, 40.7°, 58.9°, 70.2°, and 74.1° (Fig. 2d) owing to the presence of MnO, and the peaks corresponded to the (111), (200), (220), (311), and (222) reflections, respectively (JCPDS 07-0230). Moreover, the characteristic peaks for Mn_3O_4 were also observed due to the surface oxidation of MnO_x: (200), (211), (220), and (224) (JCPDS 24-0734). However, after the cascade nanoconfined synthesis of PAni, the crystal peaks of Mn-HPAni (IV, green line, Fig. 2d) disappeared. Herein, the collapse of MnO_x crystallinity indicates the change from MnO_x to Mn ions in an acidic environment. In particular, the surface of MnO_x undergoes rapid oxidation to form the Mn_3O_4 phase during the silica capping process, resulting in the MnO@Mn_3O_4 structure.[19,22] The dispersed MnO_x exhibited a light green color at high temperatures, and the color immediately became brown at ambient room temperature due to the surface oxidation of MnO_x.

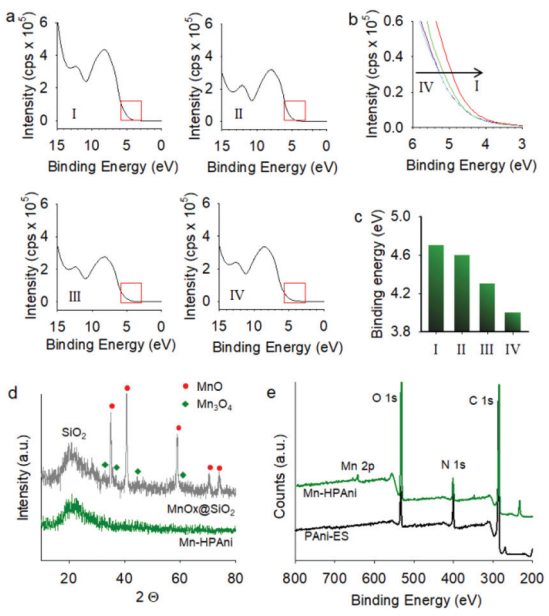

Fig. 2 Investigation of Mn-coordination state from Mn-HPAni. (a) Kinetic energy spectra of the photoelectrons for Mn-HPAni (I), Mn-HPAni (II), Mn-HPAni (III), and Mn-HPAni (IV). (b) Magnified ultraviolet photoelectron spectroscopy graph from the red boxes shown in (a). (c) Binding energy against Mn-HPAni (I–IV) nanostructures. (d) X-ray diffraction patterns of MnO_x@SiO_2 (grey line) and Mn-HPAni (IV, green line). (e) X-ray photoelectron spectroscopy of ES state (black line) and Mn-HPAni (IV, green line).

Furthermore, as demonstrated in Fig. 2e, the X-ray photoelectron spectroscopy of Mn-HPAni (IV, green line) revealed the peaks of C 1s, N 1s, and O 1s because of the presence of an aromatic amine and quinoid ring in the PAni structures of Mn-HPAni. In particular, only the Mn 2p peak was detected from the Mn-HPAni products. As expected, moreover, Mn coordination was not observed at PAni-ES.

Therefore, nanolocalized MnO_x took away electrons from the aniline monomer when the rigid nanotemplates (MnO_x) as the oxidizing agent were sacrificed by sulfuric acid and reduced to soluble Mn ions. Herein, the chemical oxidation potential of Mn_3O_4, where the surface of MnO_x is oxidized, reached 1.00 eV and that of aniline monomers is 0.7 eV.[23] Hence, the higher chemical oxidation potential induced a redox chain reaction, producing Mn-HPAni (Fig. 3). Subsequently, the aniline monomers were polymerized by oxidative polymerization around the MnO_x nanotemplate, which simultaneously leads to the formation of Mn-coordinated PAni (Mn-HPAni). Mn-HPAni might be synthesized until the complete reduction and dissolution of MnO_x. Finally, Mn-HPAni nanostructures were synthesized by MnO_x-mediated catalytic polymerization, and the hollow interior of MnO_x cores was created by acid-etching. MnO_x was used not only as the oxidant agent to polymerize aniline molecules, but also the coordinate (doping) agent for controlling the bandgap for PAni.

To evaluate the *in vitro* photothermal ablation capacity of Mn-HPAni, MKN45—a gastric cancer cell line—was treated with Mn-HPAni and then exposed to a NIR laser (λ = 808 nm, 2.45 W cm^{-2}) for up to 10 min. Thereafter, the cell viabilities were evaluated, simultaneously for both live cells and dead cells, using calcein AM and EthD-1 staining, respectively. Calcein AM staining is a membrane-permeant green fluorescent cell marker that is hydrolyzed by endogenous esterase, and consequently, emits fluorescence in the cytoplasm of live cells, and EthD-1 is a membrane-impermeable fluorescence dye that binds to DNA; however, upon cell death, the plasma membranes of these cells become disrupted, because of which EthD-1 may enter these cells and bind to the DNA within such

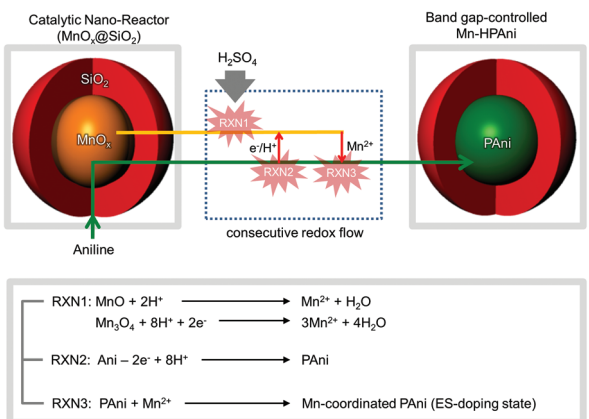

Fig. 3 Schematic of the proposed synthesis mechanism for bandgap-controlled Mn-HPAni from the catalytic nanoreactor MnO_x@SiO_2 *via* Mn-mediated catalytic polymerization.

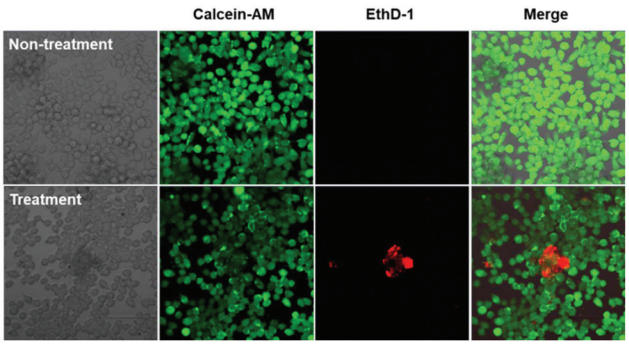

Fig. 4 Fluorescence microscopic images of MKN45 cells stained with calcein-AM and EthD-1 after NIR laser irradiation (λ = 808 nm, 2.45 W cm^{-2}) for 10 min treatment with Mn-HPAni.

cells. After 10 min of NIR laser treatment, significant cell death (EthD-1, red fluorescence) only in the MKN45 cells treated with Mn-HPAni was obvious, while none of the control group showed distinct damage to the cells (Fig. 4).

Conclusions

In conclusion, we have developed a systemic nanoreactor to construct bandgap-controlled PAni nanostructures. The binding energy of the Mn-HPAni product was clearly confirmed by absorbance and photoelectron spectroscopies. The synthesis strategy presented here simplifies the fabrication process as it allows for systemic nanolocalized synthesis and controlling the bandgap, where various structural parameters such as the size or amount of Mn oxide could be readily controlled. Conjugated polymer PAni formed a protective layer around the nanostructure, maintaining the hollow morphology. We believe that our strategy can be extended to other conjugated polymers and various hybrid nanomaterials by controlling the metal species and amount. Furthermore, such hollow morphology will have potential applications in electromagnetic interference shielding, electronic devices, and bioengineering systems. Finally, this approach will find wide acceptance and use in the field of template-directed nanostructure synthesis. It may open up new ways to fabricate conjugated polymeric nanostructures with controllable bandgap energies.

Conflicts of interest

There are no conflicts to declare.

Acknowledgements

This work was supported by a National Research Foundation (NRF) grant funded by the Korean government, Ministry of Education and Science Technology (2017M2A2A6A01071157, 2018R1C1B6008799), BioNano Health-Guard Research Center funded by the Ministry of Science and ICT(MIST) of Korea as Global Frontier Project (H-GUARD-2013M3A6B2078946), and Korea Health Technology R&D Project through the Korea Health Industry Development Institute (KHIDI), funded by the Ministry of Health & Welfare (Hl17C2586), Republic of Korea.

Notes and references

1 A. M. Bryan, L. M. Santino, Y. Lu, S. Acharya and J. M. D'Arcy, *Chem. Mater.*, 2016, **28**(17), 5989–5998.
2 Q. Zhou and G. Shi, *J. Am. Chem. Soc.*, 2016, **138**(9), 2868–2876.
3 J. Huang, S. Virji, B. H. Weiller and R. B. Kaner, *J. Am. Chem. Soc.*, 2002, **125**, 314–315.
4 Z. Zhonghua, D. Shamu, C. Zili, D. Aobing, L. Guicun and C. Guanglei, *Small Methods*, 2018, **2**(10), 1800020.
5 N. Abu-Thabit, *J. Chem. Educ.*, 2016, **93**(9), 1606–1611.
6 J. Choi, Y. Hong, E. Lee, M.-H. Kim, D. Yoon, J. Suh, Y. Huh, S. Haam and J. Yang, *Nano Res.*, 2013, **6**, 356–364.
7 J. Luo, H. Zhang, X. Wang, J. Li and F. Wang, *Macromolecules*, 2007, **40**(23), 8132–8135.
8 S. Srilalitha, K. N. Jayayeera and S. S. Madhyendhra, *Int. J. Innov. Res. Sci. Eng. Technol.*, 2013, **2**(7), 2694–2696.
9 X.-G. Li, H.-J. Shen and M.-R. Huang, *e-polymers*, 2007, E-002.
10 J. Yang, J. Choi, D. Bang, E. Kim, E.-K. Lim, H. Park, J.-S. Suh, K. Lee, K.-H. Yoo and E.-K. Kim, *Angew. Chem., Int. Ed.*, 2011, **123**, 461–464.
11 L. Guicun, L. Yingmei, L. Yan, P. Hongrui and C. Kezheng, *Macromolecules*, 2011, **44**, 9319–9323.
12 O. P. Dimitriev, *Macromolecules*, 2004, **37**, 3388–3395.
13 Q. Huang, G. Chen and J. Liu, *Polym. Adv. Technol.*, 2014, **25**, 1391–1395.
14 C. M. S. Izumi, V. R. L. Constanitino, A. M. C. Ferreira and M. L. A. Temperini, *Synth. Met.*, 2006, **156**, 654–663.
15 O. P. Dimitriev, P. S. Smertenko, B. Stiller and L. Brehmer, *Synth. Met.*, 2005, **149**, 187–192.
16 J. Kim, J. Kim and K. Ariga, *Joule*, 2017, **1**, 1–30.
17 G. Wu, K. L. More, C. M. Johnston and P. Zelenay, *Science*, 2011, **332**, 443–447.
18 R. K. Paul, V. Vijayanathan and C. K. S. Pillai, *Synth. Met.*, 1999, **104**, 189–195.
19 J. Park, D. Bang, E. Kim, J. Yang, E.-K. Lim, J. Choi, B. Kang, J.-S. Suh, H. S. Park and Y.-M. Huh, *Eur. J. Inorg. Chem.*, 2012, **2012**, 5960–5965.
20 A. M. Harbotle, S. M. Hira, M. Josowicz and J. Janata, *Langmuir*, 2016, **32**(33), 8315–8321.
21 N. J. O. Silva, M. Karmaoui, V. S. Amaral, I. Puente-Orench, J. Campo, I. da Silva, R. Bustamante, A. Milan and F. Palacio, *Phys. Rev. B: Condens. Matter Mater. Phys.*, 2013, **87**, 224429.
22 T. Kim, E.-J. Cho, Y. Chae, M. Kim, A. Oh, J. Jin, E.-S. Lee, H. Baik, S. Haam and J.-S. Suh, *Angew. Chem., Int. Ed.*, 2011, **50**, 10589–10593.
23 L. Pan, L. Pu, Y. Shi, S. Songm, Z. Xu, R. Zhang and Y. Zheng, *Adv. Mater.*, 2007, **19**, 461–464.